Materials & Design 213 (2022) 110304

Contents lists available at ScienceDirect

Materials & Design

journal homepage: www.elsevier.com/locate/matdes

Heat treatment of binder jet printed 17–4 PH stainless steel for subsequent deposition of tribo-functional diamond-like carbon coatings

Wolfgang Tillmann [a], Nelson Filipe Lopes Dias [a,*], Dominic Stangier [a], Christopher Schaak [b,*], Simon Höges [b]

[a] Institute of Materials Engineering, TU Dortmund University, Leonhard-Euler-Straße 2, 44227 Dortmund, Germany
[b] GKN Sinter Metals Engineering GmbH, Krebsöge 10, 42477 Radevormwald, Germany

HIGHLIGHTS

- Heat treating increases the hardness of 17–4 PH from 24 to 39 HRC and improves the load-carrying capacity.
- The diamond-like carbon coatings reduce the friction and wear of binder jet printed 17–4 PH.
- The plastic deformation wear of the entire substrate/coating system is reduced by a harder 17–4 PH substrate.

GRAPHICAL ABSTRACT

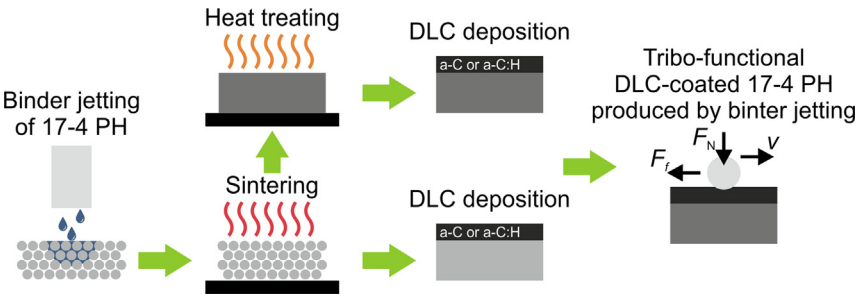

ARTICLE INFO

Article history:
Received 27 July 2021
Revised 22 November 2021
Accepted 4 December 2021
Available online 6 December 2021

Keywords:
Additive manufacturing
Binder jetting
17–4 PH
Diamond-like carbon
Sputtering
Tribology

ABSTRACT

Diamond-like carbon (DLC) coatings deposited on additively manufactured steel greatly improve the tribological properties. However, a high substrate hardness is crucial to sustaining high mechanical loads in the tribological contact. Herein, the heat treatment of binder jet printed 17–4 PH enhances the hardness from 24 to 39 HRC. Binder jet printed 17–4 PH substrates are coated by DLC of the types hydrogen-free amorphous carbon (a-C) of ~23 GPa and hydrogenated amorphous carbon (a-C:H) of ~20 GPa. The influence of the heat treatment on the tribo-mechanical properties of the DLC coatings is investigated. 17–4 PH demonstrates high friction and wear against steel counterparts, but the wear rate is reduced from 693 ± 43 × 10^{-6} mm^3/Nm to 492 ± 41 × 10^{-6} mm^3/Nm by heat treating the steel. Both a–C and a–C:H are effective in reducing the friction and wear with wear rates below 0.3 × 10^{-6} mm^3/Nm. The a–C and a–C:H coatings demonstrate lower plastic wear on heat treated 17–4 PH due to the higher substrate hardness. Consequently, the heat treatment is an essential process step to ensure maximum tribological functionality of the DLC coating on additively manufactured 17–4 PH steel.

1. Introduction

In additive manufacturing, metal binder jetting (MBJ) enables the large-scale production of complex geometries at higher build rates and lower manufacturing costs compared to laser powder bed fusion (L-PBF) processes [1,2]. MBJ is a two-step process consisting of printing the green body and subsequently sintering it [3]. For printing, MBJ combines the powder bed process with the jetting technique. The jetting nozzles spread an agent, consisting of binder and solvent, on the build platform at the position of the part contour [4]. This procedure is repeated layer-wisely until the entire 3D contour is built. The binder bonds the powder particles into a green body. The green strength of the part is given in the curing treatment [5,6]. Thereafter, the green part must be excavated from the loose powder in a so-called "de-powdering" or "de-caking" [7]. In the final process sequence, the green parts are

* Corresponding authors.
E-mail addresses: filipe.dias@tu-dortmund.de (N.F. Lopes Dias), christopher.schaak@gknpm.com (C. Schaak).

https://doi.org/10.1016/j.matdes.2021.110304
0264-1275/

heated in a high temperature furnace, where the debinding step removes the binder and the subsequent sintering step compacts the printed part at high temperatures [8].

In the current state of MBJ, the stainless steels X2CrNiMo17-12-2 (AISI 316L) and X5CrNiCuNb16-4 (AISI 630), widely known by its name 17–4 PH, are mainly used to additively manufacture steel parts [9]. 17–4 PH is a martensitic precipitation hardening chromium-nickel-copper steel with good corrosion resistance and machinability as well as high strength, toughness, and hardness in heat treated condition [10–12]. These characteristics allow a wide variety of applications in the field of automotive, aeronautical, maritime, and medical engineering, among others. 17–4 PH is a well-established steel for metal injection molding (MIM) processes. After precipitation heat treatment, the resultant martensitic structure contains Cu-rich precipitates. Additionally, Cr-rich phase and Mn-, Ni-, and Si-rich phases can occur [13].

The deposition of a functional diamond-like carbon (DLC) coating onto additively manufactured components and parts is an effective approach to enhance the surface properties and to overcome material-based restrictions of the substrate materials. DLC is composed of an amorphous network of sp^2- and sp^3-hybridized carbon atoms, thereby providing an intermediate material behavior between diamond and graphite [14,15]. In the hydrogenated state, DLC also contains hydrogen atoms, which form C–H dangling bonds in the network. These bonds lead to a chain termination of the cross-linked structure and thus to a reduced density and hardness [16,17]. Tribological DLC coatings generally exhibit a unique combination of high hardness, low friction, high resistance against wear and corrosion, and chemical inertness [18]. Among the physical vapor deposition techniques, magnetron sputtering is widely used to deposit DLC coatings for industrial applications [19,20]. This method allows to synthesize hydrogen-free amorphous carbon (a–C) [21] and hydrogenated amorphous carbon (a–C:H) [22] as tribological coating material.

The application of DLC coatings greatly expands the use of additively manufactured components for tribologically stressed surface systems. A previous study demonstrated that DLC coatings possess a high adhesion strength on L-PBF produced 36NiCrMo16 steel and significantly increase the hardness by simultaneously reducing friction and wear [23]. For additively manufactured substrates produced by MBJ, it was shown that, independently of the density or building orientation of X2CrNiMo17-12–2 (AISI 316L), the DLC coating exhibits high adhesion, even on surface areas of high open pore density [24]. However, the deposition of DLC on binder jet printed 17–4 PH in order to improve the tribological properties was not addressed in previous investigations, although the DLC deposition expands the fields of application of additively manufactured 17–4 PH towards tribological use.

For tribological applications, a high substrate hardness is crucial to withstand high mechanical loads without the substrate/coating compound suffering a plastic deformation [25,26]. Heat treating the steel substrate is generally done to increase the substrate hardness and to improve the load-carrying capacity of the substrate material against high mechanical loads. The precipitation hardening of 17–4 PH generally consists of a solution annealing with quenching and a subsequent aging at temperatures between 480 and 760 °C [27]. For 17–4 PH produced by L-PBF, Sabooni et al. demonstrated that the heat treatment is effective in tailoring the microstructure and, thereby, achieving favorable mechanical properties [28]. For 17–4 PH printed by MBJ, Huber et al. reported that the aging temperature has a decisive influence on the hardness and tensile strength [29].

Therefore, heat treating the binder jet printed 17–4 PH steel after the sintering sequence is favorable to increase the hardness and, thereby, to provide an improved load-carrying capacity for tribo-functional DLC coatings. In as-sintered and heat treated conditions, 17–4 PH was coated with hydrogen-free a–C and hydrogenated a–C:H as DLC material type. The influence of the heat treatment of binder jet printed 17–4 PH on the mechanical properties, adhesion behavior, and tribological properties of these DLC coatings was analyzed. It was demonstrated that heat treating 17–4 PH enhances its hardness and reduces the plastic deformation of the entire substrate/coating system under tribological loads. As a consequence, the a–C and a–C:H coatings with heat treated substrates demonstrate lower wear compared to those deposited on as-sintered 17–4 PH.

2. Experimental details

2.1. Binder jetting of 17–4 PH and DLC deposition

For printing, an HP Metal Jet (HP Inc., USA) was used. This system was in a pre-production status at the time of this study. The used "Ancor AM 17–4PH 0-25 μm" powder was produced (gas atomized) and supplied by GKN Hoeganaes Corporation (Cinnaminson, NJ, USA). Table 1 depicts the chemical composition of the powder. The "Ancor AM 0–25" powders are designed for printing with binder jetting regarding the particle size fraction and the sintering activity. The mean particle size of the used powder lot is x50 = 11.09 μm (x10 = 4.38 μm, x90 = 21.18 μm) and the Hausner Ratio is 1.3. For printing 17–4 PH, a layer thickness of 50 μm is commonly used to achieve a high green and sintered density. The sintering process was conducted at a maximum sinter temperature of 1360 °C and a holding time of 2 h. With the adjusted sinter profile for 17–4 PH, a sintered density from 7.60 to 7.65 g/cm^3 can be achieved (min/max values). The precipitation heat treatment was conducted at 1020 °C for 30 min with quenching at air (solution treatment) and a second step at 480 °C for 180 min followed by air quenching. The heat treatment was chosen to achieve mechanical properties according to H900 ASTM A564 [27]. For the experiments, 17–4 PH substrates were used in the as-sintered state and H900 state. The 17–4 PH substrates were metallographically lapped and polished using a diamond suspension with a grain size of 3 and 1 μm and a SiO_2 suspension with a grain size of 50 nm for 6 min each.

The a–C and a–C:H layers were deposited with a chemically graded chromium carbide (Cr_xC_y) interlayer on the binder jet printed 17–4 PH substrates using an industrial-scale magnetron sputtering device CC800/9 Custom (CemeCon AG, Germany). One chromium (Cr) (purity 99.95%) and two graphite targets (purity 99.9%) , with each having a target size of 500 × 88 mm^2, were mounted on the cathodes. Before deposition, the 17–4 PH substrates were etched with highly ionized argon (purity 99.999%) and krypton (purity 99.999%) for 30 min. The etching parameters are provided in [30]. The Cr_xC_y interlayer of ~2 μm thickness served to improve the adhesion of the a–C(:H) layers on the 17–4 PH substrates. To obtain a chemically graded transition from Cr-rich to C-rich, the Cr and graphite targets were simultaneously sputtered, while the cathode power of the Cr target was stepwisely decreased. A detailed description of the Cr_xC_y deposition process is given in [31]. For the a–C deposition, the cathodes with the graphite targets were bipolarly pulsed with a cathode power of 2.0 kW and a mid-frequency of 20 kHz. The working pressure was set to 300 mPa in an argon-controlled atmosphere. A bias voltage of −100 V was applied on the substrates. For the a–C:H deposition, acetylene (purity 99.6%) was additionally injected into the deposition chamber with a flow rate of 15 sccm. To obtain a thickness of ~1 μm, the deposition time was set to 25,200 s and 14,200 s for a–C and a–C:H, respectively.

Table 1
Chemical composition of the "Ancor AM 17–4 PH 0–25 μm" powder.

Element [wt.-%]	Fe	Cr	Ni	Cu	Mn	Si	Nb	Mo	S	N	O	C
17–4 PH powder	bal.	16.2	4.05	3.86	0.82	0.35	0.31	<0.25	<0.25	0.10	0.08	0.04

2.2. Substrate and coating characterization

The phase composition of 17–4 PH was characterized by x-ray diffraction (XRD) using a D8 Advance diffractometer (Bruker, Germany) in Bragg-Brentano geometry. The XRD diffractograms were obtained using CuKα radiation (λ = 1.5418 Å) over the scanning range 2θ from 40° to 100° with a resolution of 0.034° per step and a step time of 1 s. The binder jet printed 17–4 PH steel was metallographically polished and etched with V2A solution (Schmitz Metallographie, Germany) and Lichtenegger-Blöch solution to analyze the microstructure. The topography of the polished 17–4 PH substrates was analyzed by scanning electron microscopy (SEM) using a JSM-7001F (JEOL Ltd., Japan). The average mean roughness R_a and mean roughness depth R_z of the uncoated 17–4 PH substrates were measured using a confocal 3D microscopy μsurf (NanoFocus GmbH, Germany). Rockwell C hardness of the 17–4 PH steel was determined by a universal hardness tester (Diatestor 2Rc, Wolpert, Germany). For determining the tensile test properties, MPIF10 samples were tested in a universal testing machine type AllroundLine 100 kN (ZwickRoell GmbH & Co. KG, Germany).

SEM analyses of the DLC coatings on 17–4 PH were carried out to examine the cross-sectional morphology and topography. The SEM micrographs were generated using secondary electron (SE) and backscattered electron (BSE) detectors. For the DLC coated 17–4 PH substrates, the roughness values R_a and R_z were also determined. The hardness and elastic modulus of the uncoated 17–4 PH substrates and DLC coatings were determined by nanoindentation using a G200 (Agilent Technology, USA) with a Berkovich diamond tip. For the DLC coatings, the penetration depth was below 10% of the coating thickness to avoid substrate effects. The elastic modulus was calculated from the indentation curves using the method proposed by Oliver and Pharr [32]. The adhesion of the DLC coatings on 17–4 PH was evaluated by Rockwell C indentation test according to DIN 4856:2018–02 [33]. The Rockwell C indents were examined by SEM and categorized into the adhesion classes HF1 (excellent adhesion) to HF6 (poor adhesion). The tribological properties of the uncoated 17–4 PH and DLC coatings were investigated using a pin-on-disc tribometer under dry condition against 100Cr6 (AISI 52100) balls of 11.3 ± 0.2 GPa hardness and 6 mm diameter. The tribometer tests were performed at a normal load of 10 N, a sliding velocity of 40 cm/s, and a total amount of 10,000 rotations in ambient atmosphere at room temperature and a relative humidity ranging from 40 to 50%. The wear rates were determined by confocal 3D microscopy and the wear mechanisms were investigated by SEM.

3. Results and discussion

3.1. Structure and mechanical properties of binder jet printed 17–4 PH

The XRD diffractograms of the binder jet printed 17–4 PH steel in as-sintered and heat treated condition are shown in Fig. 1. In the as-sintered condition, the dominant phase is the body-centered cubic Fe phase with a preferred orientation along the (101) plane at 44.6°. This corresponds to either α- or δ–ferrite structure and also to the martensitic structure (deformed body-centered cubic/tetragonal). Hence, both phases are not clear to distinguish

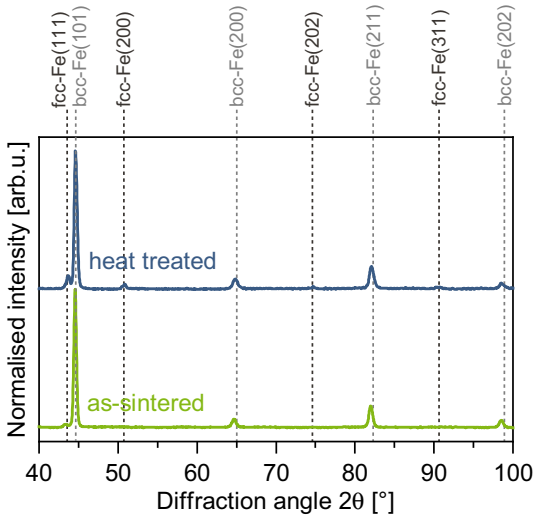

Fig. 1. X-ray diffractograms obtained from 17–4 PH produced by binder jetting in the as-sintered and heat treated condition.

from each other in the XRD diffractograms. It is well known that 17–4 PH forms δ–ferrite above a sintering temperature of 1220 °C [12]. Due to the high sintering temperature of 1360 °C in a hydrogen atmosphere, the presence of δ–ferrite can be expected. Huber et al. also identified a low fraction of δ–ferrite for binder jet printed 17–4 PH after the sintering [34]. The microstructure of the as-sintered and heat treated 17–4 PH steel is shown in Fig. 2. The microstructure shows the formation of a lighter phase along the grain boundaries, which is an indicator for δ–ferrite. This phase is typically formed along the grain boundaries. Additionally, a Bragg reflection is identified at 43.6°, which is assigned to the γ-Fe phase. The face-centered cubic γ-Fe phase indicates that austenite is already present in the as-sintered condition. However, the low intensity suggests a small amount of retained austenite. In heat treated condition, the formation of new Bragg reflections is noted at 50.7°, 74.6°, and 90.6°, which also correspond to the γ-Fe phase. Furthermore, the intensity of the Bragg reflection of γ–Fe at 43.6° increases, indicating a larger amount of austenite for heat treated 17–4 PH compared to as-sintered 17–4 PH. The increase in the amount of retained austenite after heat treating results from the reversion of martensite and δ–ferrite to austenite during the precipitation heat treatment at 1020 °C / 480 °C (see paragraph 2.1). This retained austenite occurs when the steel is not quenched to a temperature below martensite finish temperature. However, the body-centered cubic phase Fe phase with the preferred orientation at 44.6° remains dominant for the heat treated condition, demonstrating that the heat treated 17–4 PH steel consists mainly of martensite. The light micrographs of the microstructure in Fig. 2 confirm the occurrence of the three phases martensite, δ–ferrite, and retained austenite in different fractions. Martensite shows optically the highest fraction. δ–ferrite and austenite can be found along the grain's boundaries of the martensite grain. Next to the three different phases, some finely distributed residual porosity is visible. The occurrence of residual porosity is typical after sintering. Without liquid phase sintering or additional processes like hot isostatic pressing, a pore-free microstructure is hardly achieved.

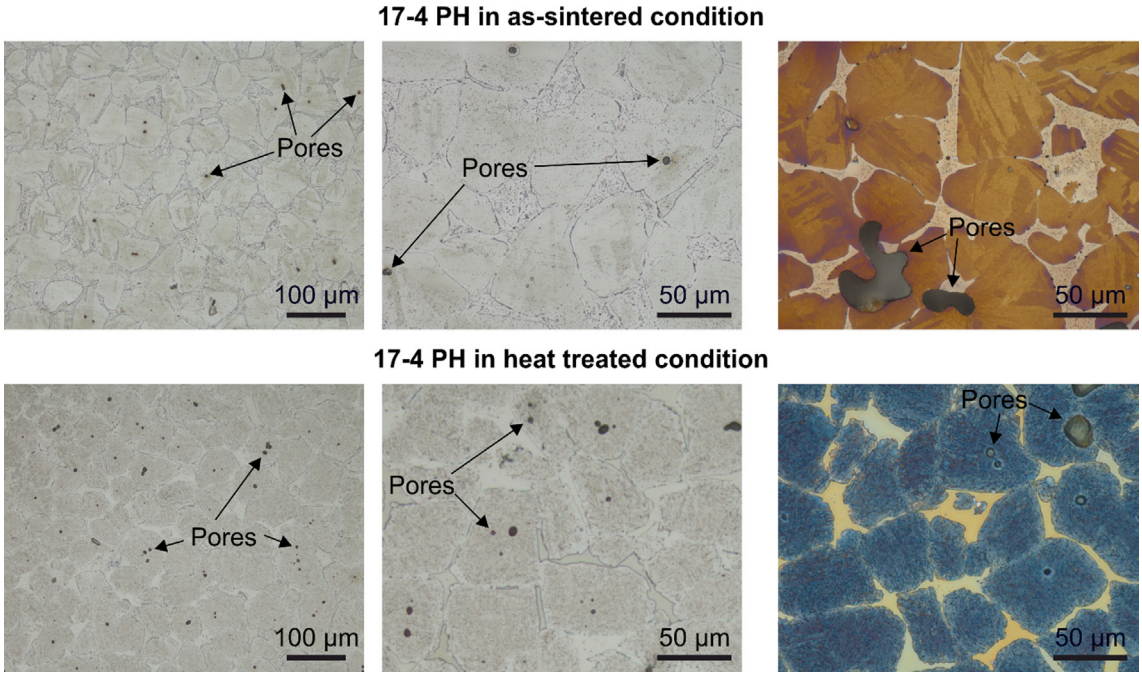

Fig. 2. Light micrographs of the microstructure of 17–4 PH produced by binder jetting in the as-sintered and heat treated condition (H900), etched by V2A (left) and Lichtenegger-Blöch (right) etching solution.

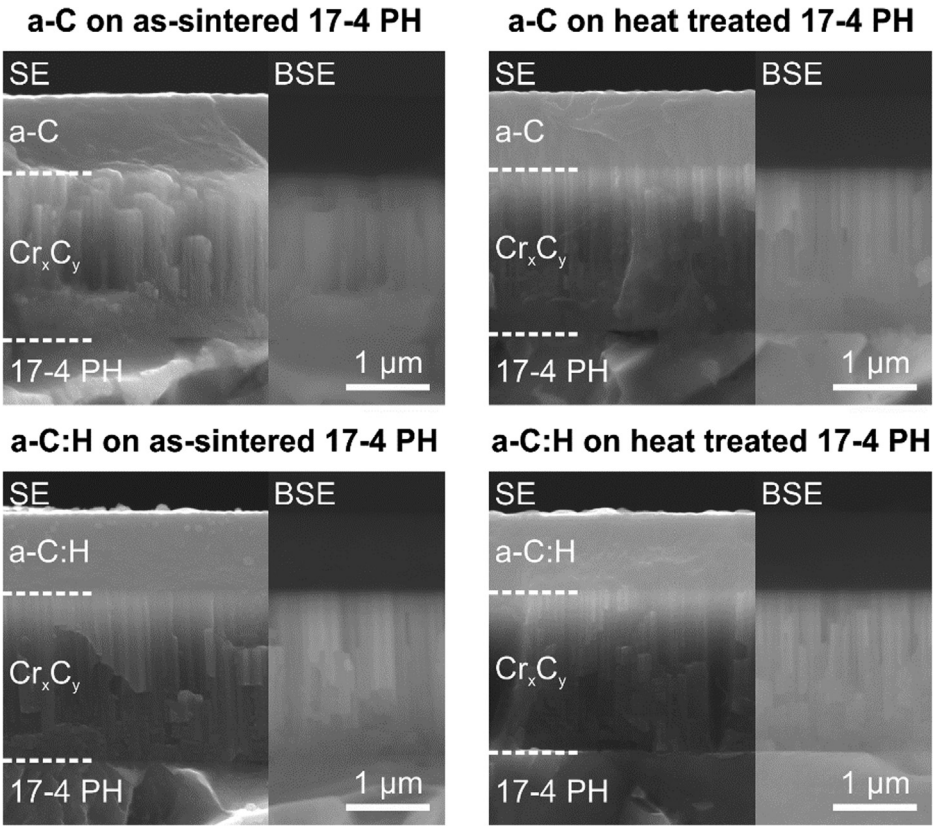

Fig. 3. Cross-sectional SEM micrographs of the morphology of the a–C(:H) coatings on 17–4 PH produced by binder jetting in the as-sintered and heat treated (H900) condition.

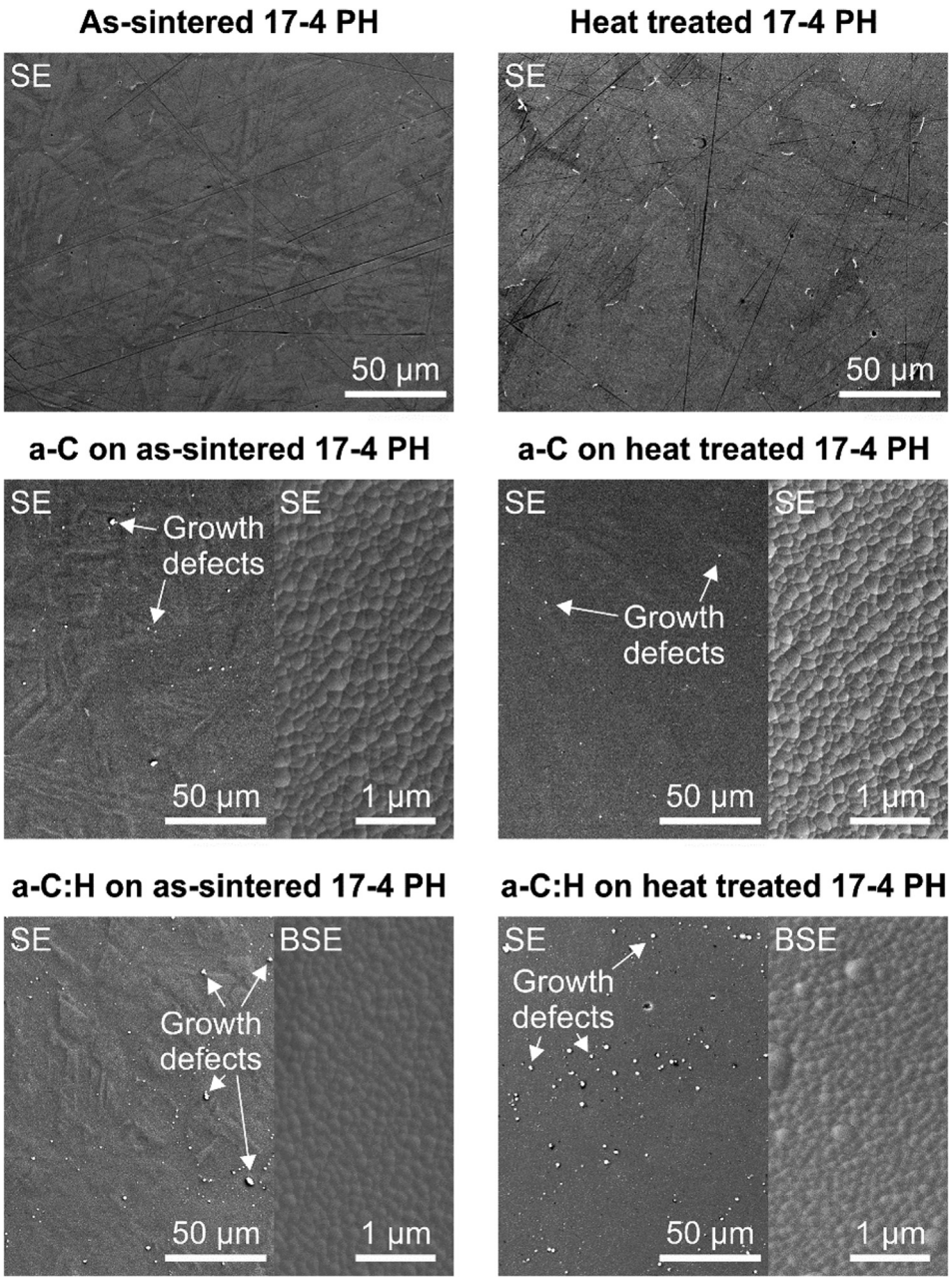

Fig. 4. SEM micrographs of the topography of uncoated 17–4 PH produced by binder jetting and a–C(:H) coatings, with 17–4 PH in the as-sintered and heat treated (H900) condition.

The SEM micrographs of the topography of the polished 17–4 PH steel are shown in Fig. 4. The scratches on the surface of the substrate originate from the polishing treatment. For the as-sintered 17–4 PH, large grains with a surrounding lighter phase are also visible on the polished surface. It is also visible that the large grains were unevenly polished, leading to irregular structures within the grains. This correlates with the lower hardness and the lower martensite amount. The heat treated 17–4 PH steel also reveals large grains embedded by a surrounding matrix on the polished surface. In the heat treated condition, the large grains seem to be more homogeneous without irregularities. This is also confirmed by the surface roughness of the 17–4 PH substrates (see Fig. 5). The as-sintered 17–4 PH steel possesses higher roughness values of R_a = 17.4 ± 0.7 nm and R_z = 97.6 ± 4.6 nm compared to heat treated 17–4 PH with R_a = 12.4 ± 1.1 nm and R_z = 67.4 ± 4.3 nm. Hence, heat treating 17–4 PH is beneficial for a more homogenous material removal during mechanical pretreatment.

With the conducted heat treatment, the hardness increased from 24 ± 1 HRC (as-sintered) to 39 ± 1 HRC (H900 state). Additionally, the ultimate tensile strength is increased around 26.4% and yield strength around 39.9%. The elongation is reduced by around 71.8%. With increased hardness, the 17–4 PH steel exhibits a more brittle material behavior.

3.2. Morphology and topography of the DLC coatings on 17–4 PH

The SEM micrographs show the coating structure consisting of the Cr_xC_y interlayer and a–C or a–C:H top layer on 17–4 PH in either as-sintered or heat treated condition (see Fig. 3). The treatment condition of the substrate does not affect the morphology of the coatings. The SEM micrographs of the topography of the a–C(:H) coatings are depicted in Fig. 4. For the coated 17–4 PH in the as-sintered structure, it is visible that both a–C and a–C:H coatings maintain the irregular structure of the substrate's large grains

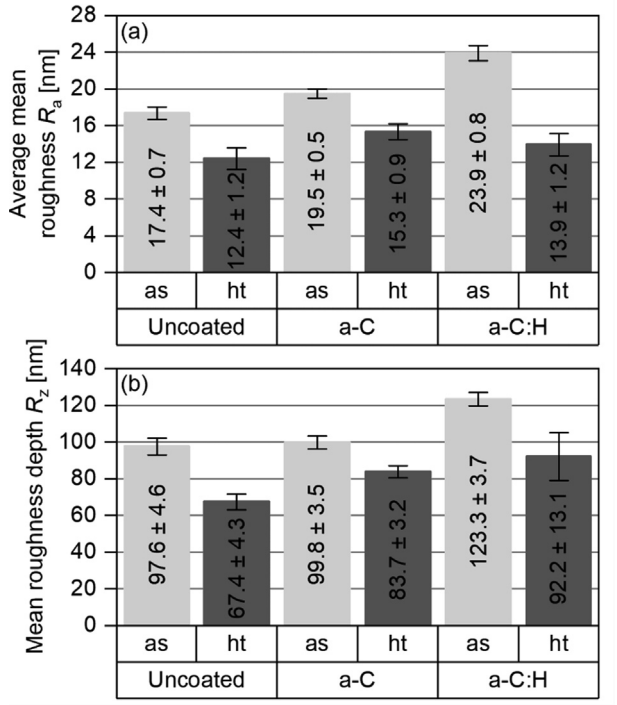

Fig. 5. (a) Average mean roughness R_a and (b) mean roughness depth R_z of uncoated 17–4 PH produced by binder jetting and a-C(:H) coatings, with 17–4 PH in the as-sintered (as) and H900 heat treated (ht) condition.

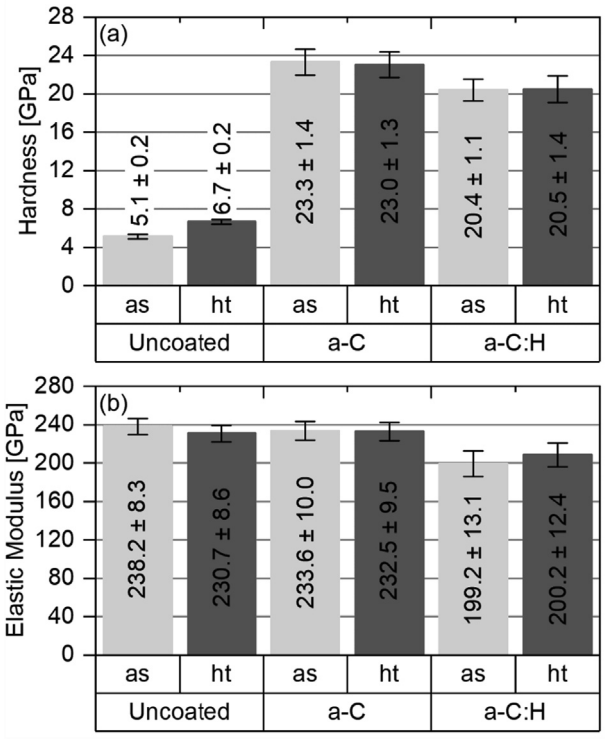

Fig. 6. (a) Hardness and (b) elastic modulus of uncoated 17–4 PH produced by binder jetting and a-C(:H) coatings, with 17–4 PH in the as-sintered (as) and H900 heat treated (ht) condition.

on the surface. Contrarily, no pronounced irregularities are observed for the same coatings on heat treated 17–4 PH due to its more homogenous surface structure.

The surface roughness of the DLC coated 17–4 PH show that the initial surface state of 17–4 PH affects the topography of the substrate/coating systems (see Fig. 5). The a–C(:H) coatings on as-sintered 17–4 PH demonstrate higher roughness values R_a and R_z compared to the respective coating on the heat treated substrate. Additionally, the DLC deposition of either a–C or a–C:H slightly increases the surface roughness. This behavior is related to the formation of growth defects (visible on the SEM micrographs of low magnification in Fig. 4), which is typical for PVD processes [35]. At higher magnification, the surface of a–C(:H) show a cluster-like structure, which is common for sputtered DLC coatings [23,30].

3.3. Mechanical properties and adhesion behavior of the DLC coatings on 17–4 PH

The hardness and elastic modulus of the uncoated 17–4–PH steel and the a–C(:H) coatings were determined by nanoindentation (see Fig. 6). The 17–4 PH steel has a hardness of 5.1 ± 0.2 GPa (in as-sintered condition, while a higher hardness of 6.7 ± 0.2 GPa is achieved by heat treating. The as-sintered and heat treated 17–4 PH substrates possess a comparable elastic modulus with values of 238.2 ± 8.3 GPa and 230.7 ± 8.6 GPa, respectively. It is worthwhile to mention that these values only represent the hardness and elastic modulus in the surface region of 17–4 PH. The macroscopic bulk hardness of the additively manufactured substrates is more appropriately described by the Rockwell C hardness (see section 3.1). The DLC coatings exhibit a significantly higher hardness than the uncoated 17–4 PH substrates. In this regard, the hydrogen-free a–C type reveals the highest hardness of ~23 GPa on both steel substrates. The hydrogenated a–C:H coating has a hardness of 20.4 ± 1.1 GPa and 20.5 ± 1.4 GPa on the as-sintered and heat treated 17–4 PH. In comparison to a–C, a lower hardness is generally identified for a–C:H due to the hydrogen. In the hydrogenated state, the coatings contain terminating C-H dangling bonds, which lower the density and hardness [16,17].

An analogous tendency is also noted for the elastic modulus of the DLC coatings, with the a–C coatings having higher values of ~230 GPa compared to a–C:H with ~200 GPa. This behavior is reported to be also attributed to a lower network rigidity caused by the C-H bonds [36]. However, the DLC coatings of either a–C or a–C:H type exhibit an elastic modulus of a comparable magnitude as that of uncoated 17–4 PH steel. For the substrate/coating system, a reduced elastic modulus mismatch between substrate and coating combined with a high coating hardness is favorable since it ensures a homogenous elastic deformation of the entire substrate/coating compound and low wear at high mechanical loads in the tribological contact [37].

The SEM micrographs of the Rockwell C indents on the a–C(:H) coated 17–4 PH substrates are shown in Fig. 7. The indents on the heat treated steel have a smaller diameter due to the higher substrate hardness. Independently of the treatment condition of 17–4 PH, both DLC coating types reveal few spalling failures of small sizes around the indent edge and are categorized into adhesion class HF2 according to DIN 4856:2018–02. Therefore, both DLC coating types exhibit good adhesion to the binder jet printed 17–4 PH steel in the as-sintered and heat treated condition. As exemplarily shown for a–C on heat-treated 17–4 PH, the coating also reveals a good adhesion on surface areas with open porosity. A similar behavior was previously reported by the authors for a–C coatings on binder jet printed X2CrNiMo17-12-2 (AISI 316L) [24]. The high adhesion strength of both coating systems results from the adjusted coating design with the chemically graded Cr_xC_y interlayer, which significantly improves the adhesion on steel substrates.

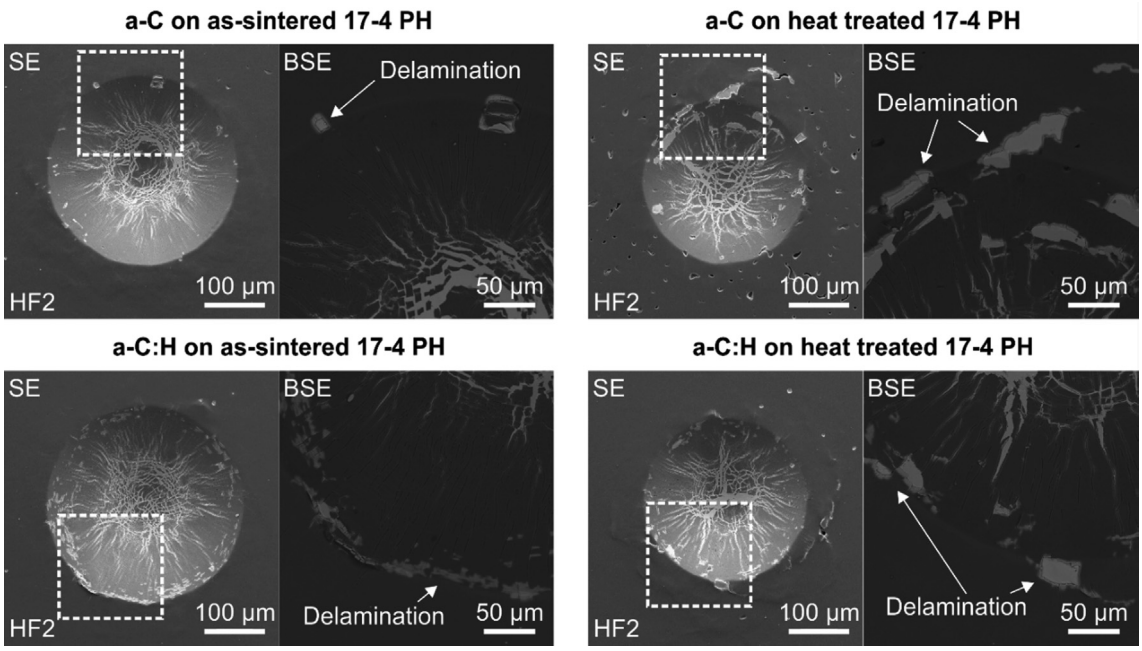

Fig. 7. SEM micrographs of Rockwell C indents performed on a–C(:H) coated 17–4 PH produced by binder jetting in the as-sintered and heat treated (H900) condition.

3.4. Tribological properties of uncoated and DLC coated 17–4 PH

The tribological properties of the uncoated 17–4 PH steel and a–C(:H) coatings were analyzed in dry sliding condition against 100Cr6 counterparts. The coefficients of friction (COF) of the different substrate/coating systems are shown in Fig. 8 (a). The as-sintered 17–4 PH steel exhibits a COF of 0.65 ± 0.06, whereas the heat-treated 17–4 PH substrate has a COF of 0.60 ± 0.01. Hence, the treatment condition of the binder jet printed 17–4 PH does not affect the friction behavior. High friction conditions are typical for steel-to-steel surfaces in dry sliding condition. Both types of a–C and a–C:H coatings significantly reduce the friction against 100Cr6 with COF values ranging from 0.226 to 0.234. The low friction is attributed to the self-generated lubricious behavior of DLC [38]. The COF of the DLC coatings is neither affected by the substrate condition of 17–4 PH nor the surface roughness in this tribometer test condition. It is assumed that the present differences in roughness do not influence the friction-reducing effect of the DLC coatings.

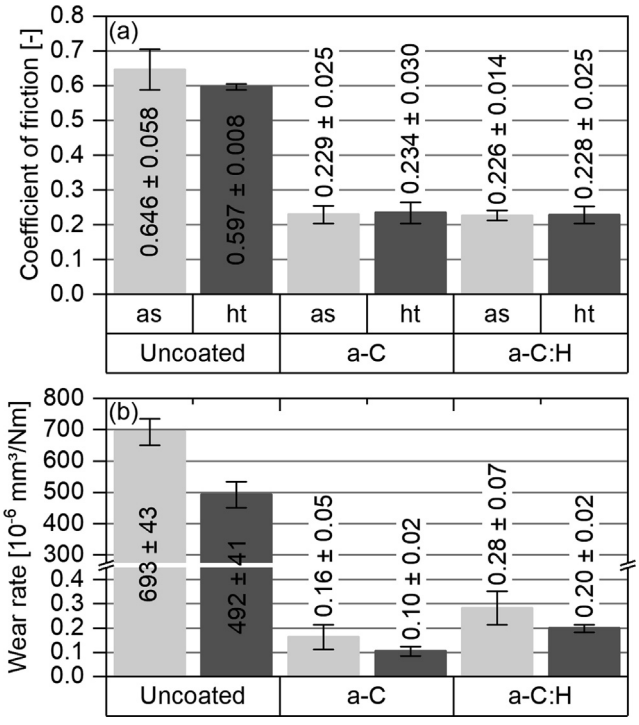

Fig. 8. (a) Coefficient of friction and (b) wear rate of uncoated 17–4 PH produced by binder jetting and a–C(:H) coatings, with 17–4 PH in the as-sintered (as) and H900 heat treated (ht) condition.

The wear rates of the uncoated and DLC coated 17–4 PH substrates are presented in Fig. 8 (b). Additionally, the 3D confocal microscopic profiles and SEM micrographs of the wear tracks are shown in Fig. 9 and Fig. 10, respectively. The uncoated 17–4 PH substrates reveal high wear rates due to excessive abrasive wear. The SEM micrographs show abrasive furrows in sliding direction. In dry contact, high wear is usually observed for either conventionally manufactured or additively manufactured 17–4 PH against 100Cr6 counterparts [39]. The heat treatment of 17–4 PH reduces the wear, leading to a lower wear rate of 492 ± 41 × 10^{-6} mm^3/Nm compared to the as-sintered substrate with 693 ± 43 × 10^{-6} mm^3/Nm. The improved wear resistance of the heat treated 17–4 PH is related to the higher hardness and, hence, to the higher resistance against abrasive wear. For conventionally manufactured 17–4 PH, Bressan et al. also reported that a high hardness ensures low wear [40].

The DLC deposition of either a–C or a–C:H significantly reduces the wear of the additively manufactured 17–4 PH with wear rates below 0.3 × 10^{-6} mm^3/Nm. The obtained results show two tendencies for the wear behavior. Firstly, the hydrogen-free a–C coatings demonstrate lower wear rates compared to a–C:H on the same substrate, which is attributed to the higher coating hardness of a–C. Secondly, it is noted that a–C and a–C:H deposited onto as-sintered 17–4 PH possess higher wear rates of 0.16 ± 0.05 × 10^{-6} mm^3/Nm and 0.28 ± 0.07 × 10^{-6} mm^3/Nm compared to a–C and a–C:H on heat-heated steel with values of 0.10 ± 0.02 × 10^{-6} mm^3/Nm and 0.20 ± 0.02 × 10^{-6} mm^3/Nm. The profiles of the wear tracks demonstrate deeper wear grooves for the coatings on the as-sintered 17–4 PH compared to the ones on the heat treated steel. However,

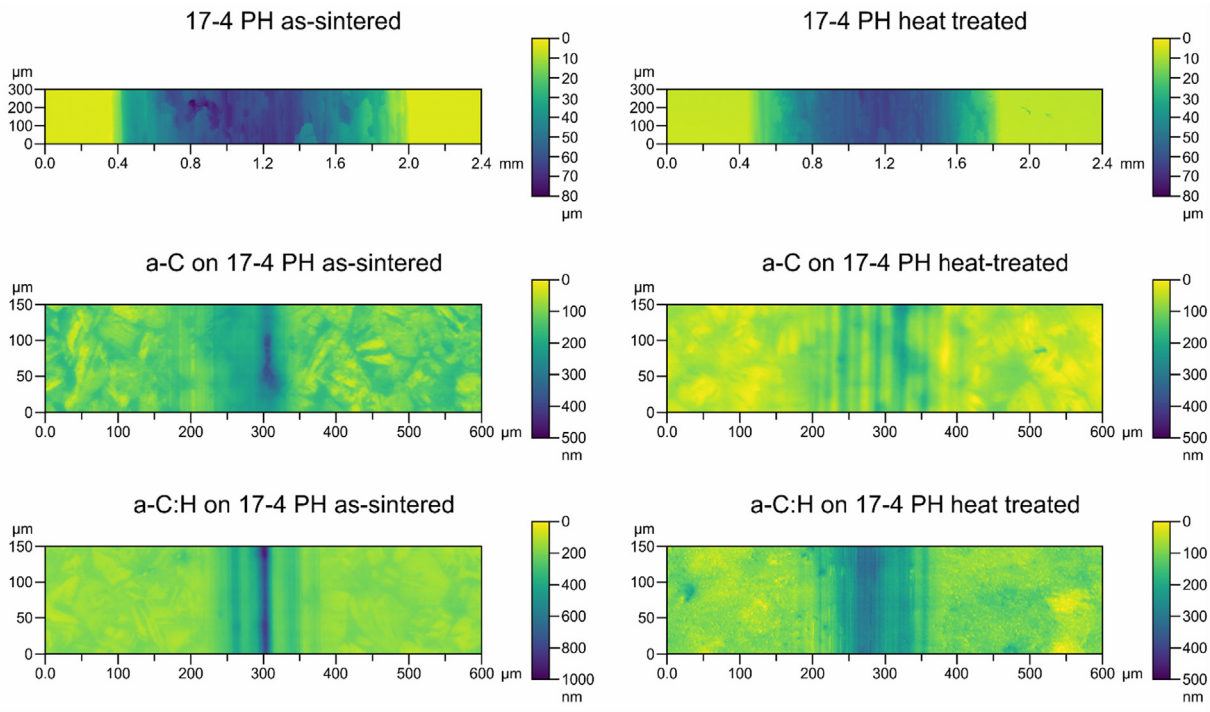

Fig. 9. 3D confocal microscopic profiles of the wear tracks of uncoated 17–4 PH produced by binder jetting and a-C(:H) coatings, with 17–4 PH in the as-sintered and heat treated (H900) condition.

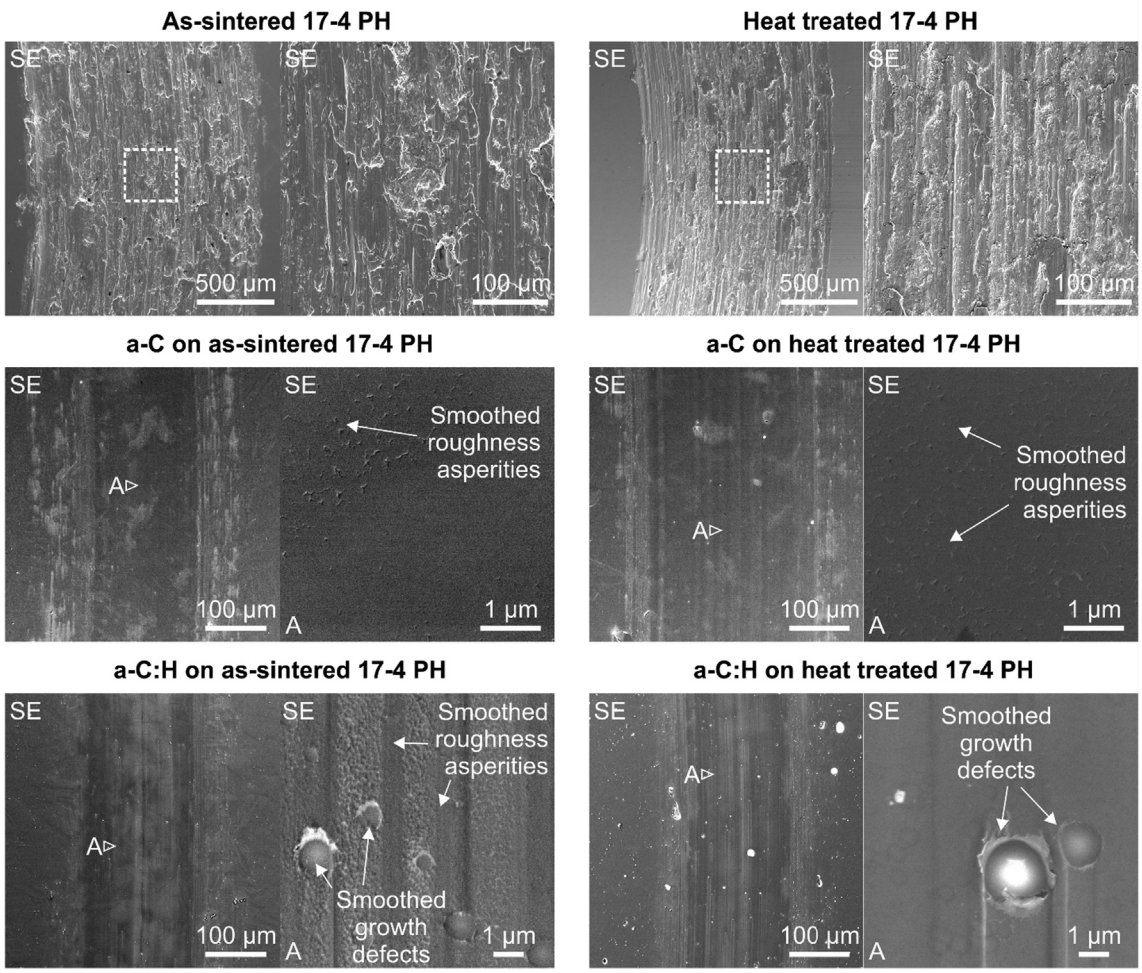

Fig. 10. SEM micrographs of the wear tracks of uncoated 17–4 PH produced by binder jetting and a-C(:H) coatings, with 17–4 PH in the as-sintered and heat treated (H900) condition.

the SEM micrographs reveal that the DLC coatings on both 17–4 PH substrates were mainly exposed to a deformative wear than rather abrasive wear since no excessive removal of the DLC coating could be observed. This is particularly evidenced by smoothed roughness asperities or growth defects along the wear track. This suggests that the wear grooves of the DLC coated 17–4 PH substrates do not only result from an abrasive and deformative wear of the DLC layer, but rather from a deformation of the entire substrate/coating system. Due to the lower substrate hardness, the 17–4 PH steel in the as-sintered condition is subjected to a higher deformation than the heat treated substrate. This explains the deep furrows along the wear tracks for the DLC coatings on as-sintered 17–4 PH, although SEM analyses show no removal of the a–C and a–C:H layer. Therefore, the obtained wear rates do not solely stem from abrasive wear, but rather from a high degree of plastic deformation leading to wear. It is also noted that hydrogen-free a–C coatings exhibit lower wear rates than hydrogenated a–C:H on 17–4 PH with its respective substrate condition. This behavior is attributed to the higher wear resistance of a–C due to its higher hardness compared to a–C:H. Hence, the DLC coatings reduce abrasive wear, whereas the substrate is responsible for the load-carrying capability. Consequently, high hardness of the additively manufactured 17–4 PH substrate is crucial for the substrate/coating system to sustain a low degree of plastic deformation under high mechanical loads.

4. Conclusions

The high hardness of the additively manufactured 17–4 PH steel substrate is essential to support the DLC coating against mechanical loads in the tribological contact. The heat treatment of 17–4 PH produced by binder jetting improves the load-carrying capacity by increasing the substrate hardness from 24 ± 1 HRC to 39 ± 1 HRC. The hardness increase is related to the higher fraction of martensite and the precipitation hardening. The DLC coatings of hydrogen-free a–C and hydrogenated a–C:H types exhibit a hardness of ∼23 GPa and ∼20 GPa and possess a high adhesion on 17–4 PH, independently of the substrate condition. The uncoated 17–4 PH steel reveals high friction with COF values of 0.65 ± 0.06 and 0.60 ± 0.01 as well as high abrasive wear against the 100Cr6 counterpart in either as-sintered or heat treated condition. However, the heat treatment reduces the wear rate of 17–4 PH from $693 \pm 43 \times 10^{-6}$ mm^3/Nm to $492 \pm 41 \times 10^{-6}$ mm^3/Nm due to the hardness increase. By applying the DLC coatings on additively manufactured 17–4 PH, the friction is lowered to COF values of ∼0.23 and the wear is significantly reduced to wear rates below 0.3×10^{-6} mm^3/Nm. The wear behavior of the DLC coated 17–4 PH steel is affected by both the type of a–C or a–C:H coating and substrate hardness. On the one hand, the hydrogen-free a–C layer reveals a higher wear resistance than hydrogenated a–C:H due to its higher hardness. On the other hand, the heat treated 17–4 PH steel ensures a lower plastic deformation of the entire substrate/-coating system. Therefore, the heat treatment of additively manufactured 17–4 PH is crucial to improve its load-carrying capability and, thereby, to fully exploit the advantageous properties of DLC for tribological applications. This approach allows to produce complex-shaped 17–4 PH components with enhanced tribological properties, which can be used as friction-reducing and wear-resistant machine elements in tribological applications. In this field, the entire manufacturing route, consisting of additive manufacturing, heat treatment, DLC deposition, as well as pre- and post-treatments, needs to be considered and closely adjusted to each other in order to produce substrate/coating systems with enhanced tribological properties.

CRediT authorship contribution statement

Wolfgang Tillmann: Resources, Writing – review & editing, Supervision. **Nelson Filipe Lopes Dias:** Conceptualization, Methodology, Investigation, Writing – original draft, Visualization, Project administration. **Dominic Stangier:** Validation, Methodology, Investigation, Writing – review & editing, Supervision. **Christopher Schaak:** Conceptualization, Methodology, Investigation, Resources, Writing – original draft, Supervision, Project administration. **Simon Höges:** Resources, Writing – review & editing, Supervision.

Declaration of Competing Interest

The authors declare that they have no known competing financial interests or personal relationships that could have appeared to influence the work reported in this paper.

Acknowledgments

The authors would like to thank Mr. Fabian Behrenberg from the Institute of Materials Engineering (TU Dortmund University) for conducting the metallographic preparation and white light microscopic investigations. The authors would also like to thank Prof. Dr.-Ing. Dirk Biermann and Alexander Meijer from the Institute of Machining Technology (TU Dortmund University) for providing the confocal 3D microscope.

Data availability

The raw data required to reproduce these findings are available upon request.

References

[1] M. Ziaee, N.B. Crane, Binder jetting: a review of process, materials, and methods, Addit. Manuf. 28 (2019) 781–801, https://doi.org/10.1016/j.addma.2019.05.031.
[2] A. Mostafaei, A.M. Elliott, J.E. Barnes, F. Li, W. Tan, C.L. Cramer, P. Nandwana, M. Chmielus, Binder jet 3D printing – Process parameters, in: materials, properties, and challenges, Progress in Materials Science, 2020, p. 100707, https://doi.org/10.1016/j.pmatsci.2020.100707.
[3] L. Yang, K. Hsu, B. Baughman, D. Godfrey, F. Medina, M. Menon, S. Wiener, Additive Manufacturing of Metals: The Technology, Materials, Design and Production (2017). DOI: 10.1007/978-3-319-55128-9.
[4] A. Lores, N. Azurmendi, I. Agote, E. Zuza, A review on recent developments in binder jetting metal additive manufacturing: materials and process characteristics, Powder Metall. 62 (5) (2019) 267–296, https://doi.org/10.1080/00325899.2019.1669299.
[5] M. Salehi, M. Gupta, S. Maleksaeedi, N.M.L. Sharon, Inkjet Based 3D Additive Manufacturing of Metals, Materials Research Forum LLC (2018).
[6] M. Leary, Design for Additive Manufacturing, Elsevier, 2020.
[7] I. Gibson, D. Rosen, B. Stucker (Eds.), Additive Manufacturing Technologies, Springer New York, New York, NY, 2015.
[8] J.O. Milewski, Additive Manufacturing of Metals, Springer International Publishing, Cham, 2017.
[9] AMPOWER GmbH & Co. KG, AMPOWER Report 2020, 2020. https://additive-manufacturing-report.com/technology/binder-jetting/#006 (accessed 23 September 2020).
[10] J.R. Davis, Stainless steels, second. printing, ASM International, Materials Park, Ohio, 1996.
[11] R.M. German, MIM 17–4 PH Stainless Steel: Processing, properties and best practice, Powder Injection Moulding International (2018) 49–76.
[12] D.C. Blaine, Y. Wu, C.E. Schlaefer, B. Marx, R.M. German, Sintering Shrinkage and Microstructure Evolution during Densification of aMartensitic Stainless Steel, 2003.
[13] G. Yeli, M.A. Auger, K. Wilford, G.D.W. Smith, P.A.J. Bagot, M.P. Moody, Sequential nucleation of phases in a 17–4PH steel: Microstructural characterisation and mechanical properties, Acta Mater. 125 (2017) 38–49, https://doi.org/10.1016/j.actamat.2016.11.052.
[14] J. Vetter, 60 years of DLC coatings: Historical highlights and technical review of cathodic arc processes to synthesize various DLC types, and their evolution for

industrial applications, Surf. Coat. Technol. 257 (2014) 213–240, https://doi.org/10.1016/j.surfcoat.2014.08.017.
[15] B. Schultrich, Tetrahedrally Bonded Amorphous Carbon Films I: Basics, Structure and Preparation, Springer Berlin Heidelberg, Berlin, Heidelberg, 2018.
[16] J. Robertson, Hydrogen in a-C, in: S.R.P. Silva (Ed.), Properties of amorphous carbon, Institution of Engineering & Technologies, London, 2008, pp. 13–20.
[17] J. Robertson, Classification of diamond-like, in: C. Donnet, A. Erdemir (Eds.), Tribology of Diamond-Like Carbon Films, Springer, US, Boston, MA, 2008, pp. 13–24.
[18] K. Bewilogua, D. Hofmann, History of diamond-like carbon films — From first experiments to worldwide applications, Surf. Coat. Technol. 242 (2014) 214–225, https://doi.org/10.1016/j.surfcoat.2014.01.031.
[19] C. Donnet, A. Erdemir, Tribology of Diamond, Diamond-Like Carbon and Related Films, in: B. Bhushan (Ed.), Modern tribology handbook, Fla, CRC Press, Boca Raton, 2001, pp. 871–899.
[20] M. Hori, Introduction to diamond-like carbons, in: Y. Kawai, H. Ikegami, N. Sato, A. Matsuda, K. Uchino, M. Kuzuya, A. Mizuno (Eds.), Industrial Plasma Technology: Applications from Environmental to Energy Technologies, Wiley-VCH Verlag GmbH & Co. KGaA, Weinheim, Germany, 2010, pp. 275–276, https://doi.org/10.1002/9783527629749.ch22.
[21] W. Tillmann, N.F. Lopes Dias, D. Stangier, M. Bayer, H. Moldenhauer, J. Debus, M. Schmitz, U. Berges, C. Westphal, Interaction effects of cathode power, bias voltage, and mid-frequency on the structural and mechanical properties of sputtered amorphous carbon films, Applied Surface Science 487 487 (2019) 857–867, https://doi.org/10.1016/j.apsusc.2019.05.131.
[22] W. Tillmann, H. Ulitzka, N.F. Lopes Dias, D. Stangier, C.A. Thomann, H. Moldenhauer, J. Debus, Effects of acetylene flow rate and bias voltage on the structural and tribo-mechanical properties of sputtered a-C: H films, Thin Solid Films 693 693 (2020) 137691, https://doi.org/10.1016/j.tsf.2019.137691.
[23] W. Tillmann, N.F. Lopes Dias, D. Stangier, L. Hagen, M. Schaper, F. Hengsbach, K.-P. Hoyer, Tribo-mechanical properties and adhesion behavior of DLC coatings sputtered onto 36NiCrMo16 produced by selective laser melting, Surface and Coatings Technology 394 394 (2020) 125748, https://doi.org/10.1016/j.surfcoat.2020.125748.
[24] W. Tillmann, N.F. Lopes Dias, D. Stangier, C. Schaak, S. Höges, Coatability of diamond-like carbon on 316L stainless steel printed by binder jetting, Addit. Manuf. 44 (2021) 102064, https://doi.org/10.1016/j.addma.2021.102064.
[25] K. Holmberg, A. Matthews, Tribological Properties of Metallic and Ceramic Coatings, in: B. Bhushan (Ed.), Modern tribology handbook, Fla, CRC Press, Boca Raton, 2001, pp. 827–870.
[26] Y. Sun, A. Bloyce, T. Bell, Finite element analysis of plastic deformation of various TiN coating/ substrate systems under normal contact with a rigid sphere, Thin Solid Films 271 (1-2) (1995) 122–131, https://doi.org/10.1016/0040-6090(95)06942-9.
[27] ASTM International, Specification for Hot-Rolled and Cold-Finished Age-Hardening Stainless Steel Bars and Shapes, West Conshohocken, PA, 2013.
[28] S. Sabooni, A. Chabok, S. Feng, H. Blaauw, T.C. Pijper, H.J. Yang, Y.T. Pei, Laser powder bed fusion of 17–4 PH stainless steel: a comparative study on the effect of heat treatment on the microstructure evolution and mechanical properties, Addit. Manuf. (2021), https://doi.org/10.1016/j.addma.2021.102176 102176.
[29] D. Huber, P. Stich, A. Fischer, Heat Treatment of 17–4 PH Stainless Steel Produced by Binder Jet Additive Manufacturing (BJAM) from N2-Atomized Powder, Prog Addit Manuf 4 (2021) 295, https://doi.org/10.1007/s40964-021-00224-z.
[30] W. Tillmann, N.F. Lopes Dias, D. Stangier, W. Maus-Friedrichs, R. Gustus, C.A. Thomann, H. Moldenhauer, J. Debus, Improved adhesion of a-C and a-C: H films with a CrC interlayer on 16MnCr5 by HiPIMS-pretreatment, Surface and Coatings Technology 375 375 (2019) 877–887, https://doi.org/10.1016/j.surfcoat.2019.07.076.
[31] W. Tillmann, N.F. Lopes Dias, D. Stangier, A. Nienhaus, C.A. Thomann, A. Wittrock, H. Moldenhauer, J. Debus, Effect of the bias voltage on the structural and tribo-mechanical properties of Ag-containing amorphous carbon films, Diamond and Related Materials 105 105 (2020) 107803, https://doi.org/10.1016/j.diamond.2020.107803.
[32] W.C. Oliver, G.M. Pharr, An improved technique for determining hardness and elastic modulus using load and displacement sensing indentation experiments, J. Mater. Res. 7 (6) (1992) 1564–1583, https://doi.org/10.1557/JMR.1992.1564.
[33] German Institute for Standardization DIN, DIN 4856:2018-02: Carbon-based films and other hard coatings - Rockwell penetration test to evaluate the adhesion, 2018.
[34] D. Huber, L. Vogel, A. Fischer, The effects of sintering temperature and hold time on densification, mechanical properties and microstructural characteristics of binder jet 3D printed 17–4 PH stainless steel, Addit. Manuf. 46 (2021) 102114, https://doi.org/10.1016/j.addma.2021.102114.
[35] P. Panjan, A. Drnovšek, P. Gselman, M. Čekada, M. Panjan, Review of Growth Defects in Thin Films Prepared by PVD Techniques, Coatings 10 (2020) 447, https://doi.org/10.3390/coatings10050447.
[36] J. Robertson, Mechanical properties and structure of diamond-like carbon, Diam. Relat. Mater. 1 (5-6) (1992) 397–406, https://doi.org/10.1016/0925-9635(92)90137-D.
[37] X. Huang, I. Etsion, T. Shao, Effects of elastic modulus mismatch between coating and substrate on the friction and wear properties of TiN and TiAlN coating systems, Wear 338–339 (2015) 54–61, https://doi.org/10.1016/j.wear.2015.05.016.
[38] J. Fontaine, C. Donnet, A. Erdemir, Fundamentals of the Tribology of DLC Coatings, in: C. Donnet, A. Erdemir (Eds.), Tribology of Diamond-Like Carbon Films, Springer, US, Boston, MA, 2008, pp. 139–154.
[39] S. Kc, P.D. Nezhadfar, C. Phillips, M.S. Kennedy, N. Shamsaei, R.L. Jackson, Tribological behavior of 17–4 PH stainless steel fabricated by traditional manufacturing and laser-based additive manufacturing methods, Wear 440–441 (2019), https://doi.org/10.1016/j.wear.2019.203100 203100.
[40] J.D. Bressan, D.P. Daros, A. Sokolowski, R.A. Mesquita, C.A. Barbosa, Influence of hardness on the wear resistance of 17–4 PH stainless steel evaluated by the pin-on-disc testing, J. Mater. Process. Technol. 205 (1-3) (2008) 353–359, https://doi.org/10.1016/j.jmatprotec.2007.11.251.